EXPLORING CUSP-CORE TRANSFORMATION

Author:
María García Gumbao

Tutors:
Chris Brook & Claudio Dalla Vecchia

Universidad de la Laguna
Master en Astrofísica

Contents

Resumen

El trabajo realizado en este proyecto consiste en estudiar la formación y evolución de una galaxia aislada, bajo el paradigma del modelo ΛCDM y utilizando el código EAGLE (una versión modificada del código de simulación Gadget). Con el objetivo de analizar el problema que se encuentra en este modelo con los perfiles de densidad de la materia oscura en las regiones centrales (*cusp-core discrepancy*), hemos ejecutado una serie de simulaciones entre las que varían diferentes parámetros encargados de describir la física detrás del comportamiento de los bariones.

Este es uno de los problemas que todavía presenta el modelo ΛCDM, que para galaxias enanas predice un perfil de densidad para la materia oscura que no se corresponde con lo que indican las observaciones. Mientras que observaciones obtenidad mediante curvas de velocidad obtienen un perfil central plano, el modelo predice un perfil de Navarro, Frenk & White, que da una sobredensidad en la región central.

El procedimiento a seguir es el siguiente: utilizamos el modelo ΛCDM para generar una sobredensidad inicial que colapse al *redshift* que a nosotros nos interesa ($z = 4$). Esta sobredensidad consistirá en una distribución esférica de partículas tanto de materia oscura como de gas, que siguen un perfil de densidad inicial $\propto 1/r$, a las cuales se le añade una velocidad inicial con tres componentes: Flujo de Hubble, necesario para simular la expansión del Universo, rotación en forma de sólido rígido, para imitar el efecto de los torques de marea que provienen de las estructuras a gran escala, y una componente gaussiana, que añade aleatoriedad. La contribución en masa de cada componente (gas o materia oscura) se establece según los parámetros cosmológicos o el parámetro f_{gas}, que permite fijar la fracción de masa que corresponde al gas, en el caso en que se deje la fracción que corresponde con la cosmología este parámetro toma el valor 0.16.

Estas condiciones iniciales se introducen al código *GADGET*, en su versión modificada para el proyecto EAGLE, un código en paralelo de tipo TreeSPH, que nos permite estudiar a partir de ese sistema cómo evoluciona la galaxia.

Los parámetros que modificamos entre las distintas simulaciones son:

- Fracción de masa constituida por el gas (f_{gas}).
- Tiempo que tarda en liberarse la energía de las supernovas de tipo II (t_{SNII}).
- Eficiencia de la formación estelar, este cambio se produce controlando el *feedback* generado por la formación estelar, mediante la normalización (A) de la ley de formación estelar de Kennicutt-Schmidt.
- Ecuación de estado. Hay tres parámetros en la simulación que contribuyen a la ecuación de estado, pero sólo modificaremos el valor umbral de la densidad ($n_{H,EOS}$), el cual establece un límite hasta el cual se aplica la ecuación de estado ideal.
- Límite en la densidad para la formación estelar ($n_{H,sf}$), valor mínimo para el que se considera que se puede producir la fase fría necesaria para que se produzca formación estelar.
- Temperatura asociada a las supernovas de tipo II (T_{SNII}), establece cuánto se calientan las partículas afectadas por la SN y cuántas son las partículas afectadas.
- Resolución, el parámetro que limita la resolución (*softening*) está fijado por las condiciones iniciales, pero se puede aumentar la resolución aumentando el número de partículas,

Mientras que muchos grupos consiguen formar núcleos de materia oscura introduciéndo bariónes y los efectos de la retroalimentación (*feedback*) que se producen, las simulaciones de EAGLE suelen hallar un perfil en forma de cúspide, incluso con la presencia de bariones, lo cual podemos observar en los resultados para el cass estándar.

En general, para las simulaciones ejecutadas con EAGLE se obtiene una historia de formación estelar suave, si la comparamos con la observada en otras simulaciones. Sabemos que una historia de formación estelar más irregular produce flujos de gas hacia el exterior, lo cual sabemos es importante en la formación de núcleos. Intentando entender las diferencias de EAGLE en la formación de núcleos hemos encontrado que varios parámetros modifican el perfil de densidad, pero ningún parámetro es capaz de producir un cambio drástico.

Los parámetros que permiten un perfil más plano el de NFW son el tiempo de retardo de las SNII, el límite de densidad para la ecuación de estado y la resolución. Sin embargo, si utilizamos parámetros similares a los utilizados en otras simulaciones no conseguimos que se forme un núcleo, mientras que ellos sí lo forman, tampoco observamos signos de flujos de gas, lo cual sí ocurre en su caso.

Los casos con una historia de formación estelar más irregular presentan más flujos de gas y un perfil más plano en las regiones centrales. Aunque el efecto no es drástico, el mayor cambio se observa al reducir el retardo en supernovas de tipo II, cuando hay un retraso entre la formación estelar y la emisión de $feedback$ la galaxia se hace estable frente a la formación de un núcleo. Esto puede deberse a que las estrellas contribuyen al pozo de potencial antes de que el gas sea emitido, haciendo que el cambio en el potencial sea menos brusco. Por otro lado, la temperatura de las SNII también son importantes, en EAGLE está fijada a un valor alto, lo que hace que se reparta mucha energía entre pocas partículas, en lugar de extenderse a un gran número de partículas como ocurre en otros modelos. Entonces, menos gas es expulsado de las regiones de formación estelar a otras cercanas, y por tanto, lo procesos necesarios para que se forma un núcleo no ocurren.

También hay una relación entre la formación de bulbo y de núcleo de materia oscura. Al formarse estrellas en la región más interna (cuando hay bulbo) el pozo de potencial se hace más profundo, impidiendo que se forme el núcleo de materia oscura. Quizás, por esto, el retardo de las supernovas es el parámetro más importante en este trabajo, esto puede interpretarse como que se necesitan otras formas de retroalimentación estelar. En EAGLE está modelada con una modificación de la ecuación de estado, pero nuestras simulaciones indican que esto no permite la formación de núcleos. Por otro lado, los núcleos que se consiguen formar son considerablemente más pequeños que los que se forman en otras simuaciones.

Podemos sacar la conclusión de que la principal diferencia entre EAGLE y otros códigos es el $feedback$ producido por las supernovas, y no la modelación de la formación estelar o la ecuación de estado.

Abstract

In this project we studied the effect that several parameters have in the simulation of a galaxy forming within the Λ cold dark matter (ΛCDM) model. The aim is to study the cusp-core discrepancy, one of the problems of the ΛCDM model, and to better understand whether this discrepancy can be explained by baryonic processes. To do so we use a set of parameters to modify the baryonic physics of the simulations and measure the dark matter profile, as we want to see the effect of these changes on the central density profile of the dark matter. We vary the initial gas fraction, the time delay and temperature of type II supernova (SNII) energy feedback, the normalization of the star formation and the density threshold for the star formation and for the equation of state; we also checked the standard case with a higher resolution. We find that the employed model is quite robust to variations of these parameters in terms of the dark matter density profile. We do, however, find that a high gas fraction results in a more flattened profile, along with a small delay in SNII feedback. The physical interpretation of this can be the requirement of gas inflows and outflows through the central regions, i.e. we need a relatively large gas mass to fall to the center and be expelled rapidly instead of forming a significant population of stars, which would deepen the potential well. We also comment on other parameters which are only able to get a modest flattening of the inner density profile at best, analyze other important features such as star formation history, gas mass in the center regions or the stellar density profile, and explore why this model is more robust at retaining cusps than other models that include baryonic processes.

1 Objectives

One of the main problems of the ΛCDM cosmological model is the difference between the theoretical prediction for the density profiles and what the observations tell us. Observations inferred from rotation curves show that many galaxies have flat or "cored" density profiles in their central region, whilst theoretical prediction from dark matter simulations favors a "cuspy" central region. One possible way to reconcile the theory with observations is the effects that baryons have on dark matter density profiles. The aim here is to explore what parameters of simulations that include baryonic processes of galaxy formation may influence the shape of the dark matter density profile and see if we are able to get a flat central profile. Other properties will be checked to try to understand what is the difference with other simulations, these are the star formation history, the stellar density profile and gas mass in the central regions.

These are the model's parameters that will be varied, a deeper description of each of them is done later on in the text:

- Contribution of gas to the initial mass.
- Delay time for supernova of type II, from now on t_{SNII}, the time it takes to release the feedback from SNII.
- Star formation efficiency.
- Equation of state, we will vary the limit imposed to the pressure in regions with higher density.
- Star formation density threshold, the density at which the conditions for star formation can happen.
- SNII temperature, the energy release by SNII.

- Resolution, by increasing the number of particles we are able to get a higher resolution.

This Master thesis is organized as follows. First, I'll make an introduction to the theory that motivated this work and some theory about spherical collapse in ΛCDM models. Then I'll explain how the initial conditions are created, the parameters changed and make a description of the simulation used. Finally, I'll discuss the results obtained and the conclusions of the work.

2 Introduction

2.1 ΛCDM Model

Currently, ΛCDM cosmology is widely considered to be the model that best describes our universe because it successfully match observations of the cosmic microwave background,CMB, (Plank Collaboration 2013 [24]),the abundances of hydrogen, helium, and lithium, the accelerating expansion of the universe observed in the light from distant galaxies and supernovae (Riess et al. 1999 [30]) and the large structures of the Universe (Percival, W.J. et al. 2001 [25]). Data from the past years (Plank Collaboration 2013 [24]) indicates that we live in a **flat universe** ($\Omega_k = 0$, being Ω_k the density parameter related to the curvature), meaning the density parameters for matter, radiation and dark energy behave as follows:

$$\Omega_m(t) + \Omega_r(t) + \Omega_\Lambda(t) = 1 \tag{1}$$

where Ω_m, Ω_r and Ω_Λ are the matter, radiation and dark energy density parameters and are defined in terms of a ratio of the critical density ($\rho(t)/\rho_{crit}(t)$), being ρ_{crit} the critical density, the limit value for which a matter dominated universe expands or ends up with a contraction, and given by $\rho_{crit} = 3H(t)^2/8\pi G$ (with $H(t)$ being the Hubble constant and G the gravitational constant).

The constituents of the universe at present time are 26.41% matter (22% dark matter and 4.41% baryonic matter), 75.59% dark energy (Λ) and a negligible contribution from radiation.

Observations also show that the universe is in a state of **accelerated expansion**, which means that, currently, Λ dominates the dynamical behaviour of the universe. In the past, the universe had an Einstein-de Sitter phase, where matter dominated (behaviour similar to the case where $\Omega_m \approx 1$) and the expansion was decelerating, this is clear because ρ_Λ is constant in time, where ρ_Λ is the dark energy density, and $\rho_m \propto a^{-3}$, ρ_m being the mass density for baryonic and dark matter and a being the scale factor of the universe, which is defined as $a = \dfrac{1}{1+z}$.

Another important feature of the ΛCDM cosmology is the nature of dark matter, which is thought to be cold, meaning that it consists of particles moving at non-relativistic speed. One consequence of this is that structures form hierarchically, starting with the small objects that would then merge to form the most massive ones.

This standard cosmological model is successful at explaining a range of observations such as the large scale structure of the Universe, Baryonic Acoustic Oscillations and the Cosmic microwave background radiation. However, problems at small scales, where gravity alone is not enough to explain observations, persist such as:

- Cusp-core disprepancy: Simulations predict an overdensity of dark matter in the innermost regions of galaxies, known as a "cuspy" density profile. While profiles obtained from rotation curves show that, actually, the center parts have a flattened profiles ("cored")
- Missing satellites problem: Simulations predict a larger number of small satellite galaxies orbiting galaxies like the Milky Way compared to the actual observed ones.
- The disk of satellites problem: In simulations, satellite galaxies are not found in a thin plane, whereas this has been observed both in the Milky Way and Andromeda.

- The Too-Big-Too-Fail problem: The model predict more galaxies than observed in the local universe with $M_{halo} \approx 10\ M_{\odot}$, which is above the mass where it is expected that re-ionization can prevent star formation.

Most of the problems have plausible solutions within ΛCDM. The aim of this work is to study the first one, the cusp-core discrepancy.

2.2 Navarro, Frenk & White profile

In the 80's it was thought that objects formed by hierarchical clustering from power-law spectra should show an isothermal structure ($\rho \propto r^{-2}$) in an Einstein-de Sitter universe e.g. Bertschinger (1985) [2]. if the exponent of the initial density perturbation spectra increases or the density of the universe decreases the profiles get steeper, Hoffman (1988) [12].

However, in 1988 some works started noting that cold dark matter halos showed a dependence of the slope with the radius, increasing at larger radii. Different authors found that the density profile was best described by a logarithmic slope changing slowly with radius e.g. Hernquist 1990 [11], Navarro et al. 1995 [21].

From the studies of a variety of CDM halos, using N-body simulations, Navarro, Frenk & White 1997 [20] found that the density profiles were all fit by an equation of the form:

$$\frac{\rho\,(r)}{\rho_{crit}} = \frac{\delta_c}{(r/r_s)\,(1+r/r_s)^2} \tag{2}$$

Where r_s is a scale radius and δ_c a characteristic density (dimensionless). Also, the critical density depends on the cosmology, as we saw before. They showed that this profile is universal in that it applies to dark matter halos of any mass. They also found that for low-mass halos, δ_c is larger which indicates that they collapsed at a higher redshift.

2.3 The cusp-core discrepancy

Currently, ΛCDM is the preferred cosmological model for describing our universe; however, it still faces some problems, like the prediction of high central density in DM halos, which appears to be contradicted by observational evidence.

When dark matter halos form through collisionless collapse, they adopt "cusped" density profile in the center, proportional to r^{-1}, while in the outer parts they follow a steeper slope proportional to r^{-3} (behaviour known as "NFW" after the aforementioned density profile). While simulations considering gas and stars as passive components on the DM halo evolution result in even higher density profiles due to the effects of adiabatic contraction (Blumenthal et al. 1984).

Several observations, however, indicate that galaxies have flat or "cored" density profiles in their central regions. For example, the recent THINGS survey (Walter et al. 2008 [35], Oh et al. 2011 [23]) and LITTLE THINGS survey found inner density profiles (Hunter et al. 2012) shallower than

NFW for a large fraction of dwarf galaxies, with an interior profile proportional to $r^{-0.4}$ This discrepancy between simulations and observations was first found by Moore (1996) [18]. These surveys used rotation curves to be able to obtain total mass profiles, then subtracted the contribution of gas and stars (obtained from the flux) to obtain a dark matter density profile. There are also some massive galaxies with extended diffuse stellar and gaseous disk that show relatively flat central DM density profiles (Kuzio de Naray and Spekkens 2011 [14]). For galaxy cluster, shallower-than-NFW profiles are recover once the brightest cluster galaxy stars are subtracted. All these lead to a search for a universal profile not only for DM, but for comprising stars and DM together (collisionless matter), Newman et al. 2013 [22].

Such observations find a flat or "cored" central dark matter profile, which contradicts the prediction for ΛCDM of a steep inner density profile ("cuspy"). However, it needs to be recalled that this prediction comes from dark matter only simulations. Whilst baryons only make up a relatively small fraction of the total mass of the universe, they are able to dissipate and collapse to the central regions of dark matter halos, and thus may be dynamically important in those regions. In fact, it has long been known that gas dissipation can result in adiabatic contraction of the inner dark matter (Blumenthal et al. 1984), a process that would worsen the cusp-core discrepancy. However, baryons may also act in various ways to decrease dark matter density. Some suggestions include the effects in-spiraling gas clumps heating the dark matter via dynamical friction (Mashchenko et al. 2006 [17]), or the effects of gas outflows (Navarro et al. 1996 [19], Read et al. 2006 [29], Pontzen and Governato 2014 [26]).

As explained in Pontzen & Governato (2014) [26], gas outflows from stellar feedback may have an effect on the DM distribution. Baryons and CDM can interact through gravitational forces and transfer energy, which could give energy to the DM particles, moving them to larger radii. There are two proposed mechanism for this transfer:

- The loss of kinetic energy of incoming material due to "dynamical friction", although the presence of dense in-falling clumps is necessary. The process works as follows: If gas arrives smoothly, an adiabatic contraction takes place, where gas accumulates in the center, increasing the gravitational potential and making dark matter contract. However, if the inflows are in the shape of dense, discrete chunk, dynamical friction takes place, here, a density wake appears behind these clumps, pulling them back and transferring kinetic energy into the dark matter (Pontzen and Governato 2014 [26], El-Zant et al. 2001 [8]).
- Another way of breaking the adiabatic contraction is through feedback from stellar population. A rapid starburst would suddenly eject most of the baryons, maybe over-compensating for the previous adiabatic contraction, in a way that the central DM density could be reduced. As discussed in Pontzen and Governato (2014) [26], the dark matter particles orbit around the center of the halo, where the gas is denser; when the gas is quickly removed, the particles are driven away, which means a gain of energy for the DM particles (which is not compensated if the gas flows back in). It has been shown that repeated outflows have a cumulative effect on dark matter (Read et al. 2006 [29]).

2.4 Evolution of perturbations

To explore these issues we will use simulations with initial conditions created from cosmologically motivated model of halo collapse. Here we provide the background of this model.

2.4.1 Linear theory of perturbations

We will study the linear approximation to the evolution of primeval fluctuations. If the perturbations are small we shall treat the evolution as that of a perfect fluid, since the cosmological principle states that the smooth background is a perfect fluid. Also, here we write the general equations, but one should take into account that for dark matter there is no pressure term, since it is expected to be collisionless.

The equations of motion for a perfect, collisional fluid are:

$$\frac{\partial \rho}{\partial t} = -\nabla \cdot (\rho \vec{v}) \qquad \textit{Continuity equation} \tag{3}$$

$$\frac{\partial \vec{v}}{\partial t} + (\vec{v} \cdot \nabla)\, \vec{v} = -\frac{1}{\rho}\nabla p - \nabla \phi \qquad \textit{Euler equation} \tag{4}$$

$$\triangle \phi = 4\pi G \rho \qquad \textit{Poisson equation} \tag{5}$$

where ρ is the density of the fluid, $\vec{v}$ the speed, p the pressure and ϕ is the gravitational potential.

If we consider small perturbations, ignore the terms of second order and higher and substract the zero order equations (since this is for a smooth background, which we are not interested in) we obtain the first order perturbation:

$$\frac{d}{dt}\left(\frac{\delta \rho}{\rho_0}\right) = \frac{d\delta}{dt} = -\nabla \cdot \delta \vec{v} \tag{6}$$

$$\frac{\partial \delta \vec{v}}{\partial t} + (\delta \vec{v} \cdot \nabla)\, \vec{v_0} = -\frac{\nabla \delta p}{\rho_0} - \nabla \delta \phi \tag{7}$$

$$\triangle \delta \phi = 4\pi G \delta \rho \tag{8}$$

where δ is defined as the overdensity ($\delta = \delta\rho/\rho_0$). There is a link between pressure and density if we assume the variation of the first is due to the second and not to a change in entropy:

$$c_s^2 = \frac{\delta p}{\delta \rho} \tag{9}$$

These are written in Eulerian coordinates for a static universe, which are the proper coordinates ($\vec{x}$); but to take the expansion of the background into consideration we need these equations in comoving coordinates ($\vec{r}$), which we can get with the following transformation:

$$\vec{x} = a\,(t)\, \vec{r} \tag{10}$$

This, with $\vec{g} = -\nabla_p \delta\phi$ and $\vec{v_0} = H\vec{x}$, yields the equations of motion for baryonic matter in comoving coordinates:

$$\dot{\delta} = -\nabla_c \vec{u} \tag{11}$$

$$\dot{\vec{u}} \; + \; 2H\vec{u} \; = \; \frac{\vec{g}}{a} \; - \; \frac{\nabla_c \delta p}{a^2 \rho_0} \tag{12}$$

$$\triangle_c^2 \delta\phi \; = \; 4\pi G \rho_0 \delta a^2 \tag{13}$$

where $\vec{u}$ is the perturbation in velocity in comoving coordinates:

$$\delta\vec{v} \; = \; a\,(t)\,\vec{u} \tag{14}$$

Finally, if we take a time derivative of the continuity equation and insert the Euler equation, while using the Poisson equation to write the gravity we get a linear wave equation in comoving coordinates:

$$\ddot{\delta} \; + \; 2H\dot{\delta} \; = \; 4\pi G \rho_0 \delta \; + \; \frac{c_s^2}{a^2} \nabla_c^2 \delta \tag{15}$$

Since this is a wave equation we can make the Fourier transform of it, with the wave vector being $\vec{k} \; = \; a\,(t)\,\vec{k_c}$. Thus getting the fundamental equation for the evolution of each amplitud $\delta_k(t)$:

$$\ddot{\delta_k} \; + \; 2H\dot{\delta_k} \; = \; \nabla_k \left(4\pi G \rho_0 \; + \; \vec{k_c}^{\,2} c_s^2 \right) \qquad \textit{baryonic matter} \tag{16}$$

$$\ddot{\delta_k} \; + \; 2H\dot{\delta_k} \; = \; 4\pi G \rho \nabla_k \qquad \textit{dark matter} \tag{17}$$

where the only difference in the last equation is that we have removed the pressure term, since dark matter is collisionless.

2.4.2 Growth factor

Being D the amplitude of the growing mode and a the scale factor, a solution for equation (15) for a Friedman-Robertson-Walker (FRW) metrics is given in Hamilton's paper [10].

$$g\,(a) \; = \; \frac{D\,(a)}{a} \; = \; \frac{5\Omega_m}{2} \frac{H_0^2 \; H\,(a)}{a} \int_0^a \frac{da'}{a'^3 \; H\,(a')^3} \tag{18}$$

Or, written as a function of the density parameter:

$$g\,(\Omega_m, \Omega_\Lambda) \; = \; \frac{5\Omega_m}{2} \int_0^1 \frac{da}{a^3 \; H\,(a)^3} \tag{19}$$

It is interesting to compare the particular cases of an EdS Universe model and the ΛCDM model.

$$g\,(a) \; = \; \frac{5}{2} \frac{H_0^3 a^{-3/2}}{a} \int_0^a \frac{da'}{a^3 \left(H_0 a^{-3/2} \right)^3} \; = \; 1 \qquad EdS \tag{20}$$

$$g\,(a) \; = \; \frac{5\Omega_m}{2} \frac{\sqrt{\Omega_m a^{-3} + \Omega_\Lambda}}{a} \int_0^a \frac{da'}{a'^3 \left(\Omega_m a^{-3} + \Omega_\Lambda \right)^{3/2}} \qquad \Lambda CDM \tag{21}$$

Resulting in a linear relation between a and D for the EdS model, and an equation that cannot be solved analytically for ΛCDM model. One may thus expect the two cosmologies to have different behaviours, however, this two solutions behave similarly at high redshift.

2.5 Spherical collapse model

On the basis of this model we create initial conditions which approximate the cosmological collapse of halos, allowing us to efficiently run a suite of simulations and explore a range of parameters. We use a uniform distribution of particles following a density profile $\propto r^{-1}$ of $5 \times 10^{10} M_{\odot}$. The aim is to have this initial distribution at $z = 15$, which will collapse around redshift 4. To do so, we need to understand the cosmology involved.

Linear theory itself is not enough to understand the formation of a galaxy (or any large scale structure we see today). To do so we need a more complex nonlinear theory. In this work we adopt a "spherical collapse" model.

One of the cornerstones of this theory is the *Birkhoff theorem*: If we evaluate one region of the universe with *spherical* symmetry we can consider the cosmology in that region to be independent of what is happening outside of it; meaning it would be described with the same set of equations, but characterized for that region of space.

This is crucial for the spherical collapse model, since it basically takes into account a region where there is an overdensity ($\delta > 0$) and studies its evolution.

Conceptually, what is going to happen is that this region, with a higher density than its surroundings, will expand in a different way (slower), until some point (*turn around*) in which the gravitational potential will cause the structure to start to collapse.

Keeping in mind that we have spherical symetry, then we will be working only with the radial component (R). This is in *proper* coordinates, not comoving. The density of the sphere at any point would be given by the following equation.

$$\rho\,(R,t) \;=\; \rho_b\,(R,t) \;+\; \delta\rho\,(R,t) \;=\; \rho_b\,(R,t)\,[1 \;+\; \delta\,(R,t)] \tag{22}$$

We will consider a distribution much smaller than the observable universe. Also, at first, the gravity is not expected to be particularly high. This allows us to study the dynamics using a Newtonian approach, dominated by the gravitational potential (ϕ).

$$\phi\,(R,t) \;=\; \phi_b\,(R,t) \;+\; \delta\phi\,(R,t) \;=\; -\frac{1}{2}\left(\frac{\ddot{a}}{a}\right) R^2 \;+\; \delta\phi\,(R,t) \tag{23}$$

Here, the EdS and ΛCDM models will diverge, since the first term on the right depends on Friedmann's equations. From now on we will consider the EdS Universe; in this case Friedmann's second equation gives the following relation.

$$-\frac{1}{2}\left(\frac{\ddot{a}}{a}\right) R^2 \;=\; \frac{2\pi}{3} G\rho_b \tag{24}$$

Taking this into account we can study the dynamics of a specific shell of radius R as follows (always keeping in mind the spherical symmetry).

$$\frac{d^2R}{dt^2} \;=\; -\frac{d\phi}{dt} \;=\; -\frac{4\pi}{3} G\rho_b\,(t)\,R \;-\; \frac{d\delta\phi}{dt} \;=\; -\frac{GM_b\,(R,t)}{R^2} \;-\; \frac{G\delta M\,(R,t)}{R^2} \tag{25}$$

being M_b the mass that would correspond to a certain radius if the density were that of the background.

Now, if we consider the mass inside the sphere as M_b plus a certain term, in which we use $\overline{\delta}$ as the mean density,

$$M_s \;=\; M_b(R,t) \;+\; \overline{\delta} M_b(R,t) \;=\; \left(1+\overline{\delta}\right) M_b(R,t) \tag{26}$$

Substituting this in the equation of motion an integrating we get

$$\frac{1}{2}\dot{R}^2 \;-\; \frac{G\;M_s}{R} \;=\; E \tag{27}$$

where the integration constant E is the total energy. We are only interested in the case where $E \;<\; 0$, since it is the condition that allows a collapse to happen.

The solutions to this are found in a parametric form as a function of the variable θ. The parameter increases with time, reaching the turn-around point when its value is π,

$$\begin{aligned} R \;&=\; A\,(1 \;-\; cos\theta) \\ t \;+\; T \;&=\; B\,(\theta \;-\; sin\theta) \\ A^3 \;&=\; G\;M_s\;B^2 \end{aligned} \tag{28}$$

where A and B can be obtained imposing initial conditions to the first and third equation, and T is just a constant that makes it possible to set the radius as $R \;=\; R_i$ at $t \;=\; t_i$,

$$A \;=\; \frac{R_i}{2}\frac{1 \;+\; \overline{\delta_i}}{\overline{\delta_i} \;-\; \left(\dfrac{1}{\Omega_i} - 1\right)} \tag{29}$$

$$B \;=\; \frac{1 \;+\; \overline{\delta_i}}{2H_i\Omega_i^{1/2}\left[\overline{\delta_i} \;-\; \left(\dfrac{1}{\Omega_i} - 1\right)\right]^{3/2}} \tag{30}$$

Now, we shall see what this means for each of the cases.

2.5.1 Spherical collapse in the EdS Universe

This is shown with more detail in [16]. When we consider an EdS Universe ($\Omega_i \;=\; 1$) we have that the Hubble parameter evolves as $H \;=\; 2/3t$. Using this we see that T, the constant to set the initial radius, is negligible. Hence, we have the following solution.

$$\begin{aligned} R \;&=\; A\,(1 \;-\; cos\theta) \\ t \;&=\; B\,(\theta \;-\; sin\theta) \\ A^3 \;&=\; G\;M_s\;B^2 \end{aligned} \tag{31}$$

$$A \;=\; \frac{R_i}{2}\left(\frac{1+\overline{\delta_i}}{\delta_i}\right) \tag{32}$$

$$B \;=\; \frac{3t_i}{4}\left(\frac{1+\overline{\delta_i}}{\overline{\delta_i}^{3/2}}\right) \tag{33}$$

From this and the definition of δ we can write:

$$\delta = \frac{9}{2}\frac{(\theta - sin\theta)^2}{(1 - cos\theta)^3} - 1 \tag{34}$$

And from the relation between the purely growing mode (related to δ_{lin}) and the scale factor we can get the evolution of δ_{lin}.

$$\delta_{lin} = \frac{5}{2}\delta_i \left(\frac{t}{t_i}\right)^{2/3} = \frac{3}{5}\left(\frac{3}{4}\right)^{2/3}(\theta - sin\theta)^{2/3} \tag{35}$$

Now, we will analyse the values of δ and δ_{lineal}, solving the previous equations, for the turn-around point ($\theta = \pi$) and the virialization point ($\theta = 2\pi$).

- Turn-around: $\delta \approx 4.55$, but $\delta_{lin} \approx 1.06$.
- Virialization: $\delta \approx 176.65$, but $\delta_{lin} \approx 1.686$.

This shows we have to be careful when using the linear approximation. Although this is not the aim of this part, but to compare this results with the values in the case of a ΛCDM Universe.

2.5.2 Spherical collapse in the ΛCDM model

It is not as easy to get an analytical result for a ΛCDM Universe. However, we can compare the simulations run in [16]. As we can see in Figure 2, the overdensity needed to reach the turn-around point in the ΛCDM Universe and the EdS Universe becomes quite different for lower redshifts but tends to the same value (4.55) for higher redshifts.

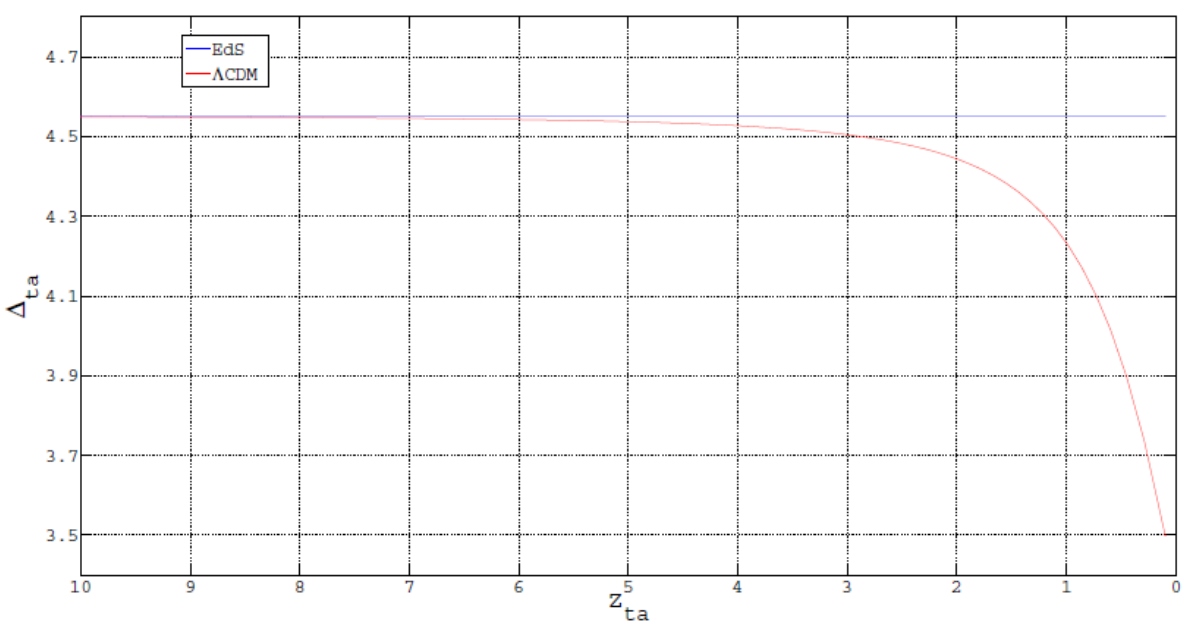

Figure 2: Overdensity versus radius for both models, obtained from the Master thesis on *Spherical Collapse in Dark Energy Models* of Robert Mardoff Nielsen (University of Oslo) [**?**] comparing the turn-around overdensity in a ΛCDM Universe and an EdS model.

Since we will be working with initial conditions in which the collapse is expected to happen at $z \approx 4$ it should not be a problem if we use the analitical results obtained for the EdS Universe even if we are studying the case of a ΛCDM Universe, the only difference it could make is that our initial distribution will collapse slightly earlier (since the turn-around overdensity used is slightly higher). The similarites of the two models is due to the fact that in a ΛCDM Universe the matter is known to dominate over the dark energy at high redshift.

3 Methodology

3.1 Initial conditions

Using the spherical collapse model we will generate an initial distribution with dark matter and gas, with a total mass of $5 \times 10^{10}\ M_{\odot}$, that will collapse at redshift 4. To do so we will consider a ΛCDM cosmology, the overdensity will be calculated using the analytical solution for an EdS simulation though, since we have explained in the introduction that the difference is not significant.

For simplicity we will use an internal system of units, which allow us to work with more manageable numbers and avoid truncation errors. For the magnitudes we are working with the system of units is defined as follows:

mass unit	$10^4\ M_{\odot}$
length unit	1 kpc
velocity unit	1 km/s

Then, The time unit is:

$$time\ unit\ = \frac{1\ kpc}{1\ km/s}\ =\ 3.0857 \times 10^{16}\ s \tag{36}$$

The ΛCDM cosmology is established setting the cosmological parameters:

- $\Omega_m = 0.2641$
- $\Omega_b = 0.0441$
- Ω_Λ = 1 - Ω_m. This means the radiation parameter is ignored and the curvature is assumed to be that of a plane.
- h = 0.7

Next, all cosmological parameters are calculated for the initial redshift ($z\ =\ 15$). Here, the EdS approximation is used when finding the initial value for the overdensity, which means, a linear dependancy is assumed.

$$\delta_i\ =\ 1.686\ \frac{a_i}{a_{col}} \tag{37}$$

Being 1.686 the overdensity at the moment of the collapse.

Given the mass of the collapsed halo, M_{200}, the radius of the collapsing initial region is given by the following equation,

$$r_{col} = \left(\frac{M_{200}}{\frac{4\pi}{3}\overline{\rho_i}\,(\delta_i + 1)} \right)^{1/3} \tag{38}$$

Particle distribution

Then the initial particle distribution is created following this algorithm:

1. Create a uniform 3D grid with as many points as particles are in the simulation.
2. Scale the distribution in a way that the density profile follows a $1/r$ distribution. This is done by multiplying each coordinate by $\sqrt{r}$.
3. Truncate the distribution at particles with a radius up to $1.1 \times r_{col}$.

This is first done with 1000 particles as a test, to calculate how many particles actually fall inside the collapse radius. Then, we can recalculate the initial number of particles in order to get that desired number of particles inside the collapse radius. After that, we can create the real particle distribution of dark matter and gas with this corrected number of particles,

$$n = \frac{n_{input}}{success\ fraction} \tag{39}$$

where the $success\ fraction$ is the fraction of the total number of particles that fall inside the collapse radius.

Masses

Up until now the mass of the particles is unknown, we can defined the total mass from the cosmological parameters as follows:

$$M_g = \frac{\Omega_b}{\Omega_m} M_{200} \tag{40}$$

$$M_{dm} = M_{200} - M_b \tag{41}$$

but we also want the possibility to change the contribution of the gas, making it different to the one establish by the cosmology, to explore the case where less than the cosmological baryon fraction are accreted into low mass halos, due to effects of UV background radiation. In that case, the mass is calculated using the parameter f_{gas}, which we will modify in the future. Then, we have that the gas mass is:

$$M_g = f_{gas}\ M_{200} \tag{42}$$

which is equal to eq. 40 when $f_{gas} = 0.16$. To know the mass of each particle we need to divide by the number of particles of that element.

Velocity distribution

Once the distribution and the masses are set, we need to add the initial velocity for the particles. This velocity is formed by three different components:

- **Hubble flow**: Since the simulation does not take into account the expansion we need to simulate it using the Hubble flow. This is calculated as follows:

$$\vec{v_{hf}} = H_i\ \vec{r}\left(1 - \frac{\delta_i}{3}\right) \tag{43}$$

- **Rotation**: To mimic the effects of tidal torques from large scale structure, we add solid body rotation to our collapsing sphere. This means that the angular velocity (ω) is constant. Using Mo, Mao and White's paper [15], we can calculate the angular momentum expected for a halo of given mass using the equation

$$J_{200} \;=\; \lambda\; M_{200}\; v_{200}\; r_{200} \tag{44}$$

where $v_{200} \;=\; (10\; G\; H_0\; M_{200})^{1/3}$ and $r_{200} \;=\; \dfrac{GM_{200}}{v_{200} * *2}$.
Therefore, the angular velocity is:

$$\omega \;=\; \frac{J_{200}}{\sum_i m_i\; r_i^2} \tag{45}$$

We add this angular velocity to the particles in our initial conditions.

- **Random velocity**: We may want to add a small random component to the velocity. This can be done creating a gaussian distribution with a dispersion of σ_v, after running some test we have chosen a value of $\sigma_v \;=\; 3\; km/s$.

We set this as the initial velocity of the particles in our initial conditions.

Internal energy

The last bit of information needed for the simulation is the internal energy of the gas elements. This is calculated considering an uniform temperature of 100 K, and that all atoms are in the neutral state.

$$u \;=\; \frac{1}{\gamma - 1}\frac{k_B\; T}{\mu\; m_H} \tag{46}$$

where γ is the adiabatic index, k_B the Boltzmann constant ($1.381 \times 10^{-23}\; J/K$), μ the mean molecular weight, m_H the mass of the Hydrogen atom and T the temperature of the gas.

Softening

The gravitational softening length is chosen to mimic those used in fully cosmological simulations. We calculate what would be the mean interparticle distance if we had box of volume $1Mpc^3$, filled with particles with the same mass as ours and the critical density as the mean density of the box.

The typical value for the softening is $1/20 - 1/50$ (Power et al. 2005 [27])of this mean free path. In our case we will use 1/50, since simulations like ours fall usually in this side of the spectrum. This will take to different values, for the standard and the high resolution cases:

- Standard: $\epsilon \;=\; 0.332$
- High resolution: $\epsilon \;=\; 0.132$

Output

Finally this information pertaining to the particles initial positions, velocities, mass and energy are written into a hdf5 file, where different groups correspond to different particles:

- Group 0: Gas.
- Group 1: Dark Matter.
- Group 4: Stars, empty in the initial conditions.

3.2 EAGLE

The code we are using to run the simulations is a modified version of *GADGET3* (this version is used in the EAGLE simulation [33]), this is a parallel Tree-SPH code. This means that it treats differently gas particles and collisionless fluids (i.e. dark matter), and also that it runs on multiple processors.

For the dark matter it works following the N-body method, while for the gas particles it uses smoothed particles hydrodynamics (SPH). It also works different with short-range and long-range forces, computing the first ones with a Tree method, and using Fourier techniques for the calculation of the later, this is usually referred to as the TreePM algorithm.

EAGLE includes physics of gravity, hydrodynamics, gas cooling, UV background radiation, star formation and supernova feedback. In detail:

- Radiative cooling: Implemented element-by-element for the following 11 elements: H, He, C, N, O, Ne, Mg, Si, S, Ca and Fe; this accounts for variations both in the metallicity and the relative abundances of the elements. The gas is assumed to be in ionization equilibrium and exposed to the cosmic microwave background (CDM), which may cause the overestimate of the cooling rate. Also, self-shielding is ignored (although it can cause an underestimation of the cooling effects).
- Reionization: The background ionization is turned on at redshift $z = 11.5$. To heat the gas at reionization, 2 eV are injected into the particles, instantly for H, and with a gaussian centered at $z = 3.5$ and $\sigma = 0.5$ for He.
- Star formation: Star formation follows the Kennicutt-Schmidt star formation law, but here it is taken to depend on pressure rather than density. A dependence on the metallicity is added to the critical volume density to model that the transition to a cold, molecular phase happens at a lower density when the metallicity is higher.
  A temperature floor is imposed because the simulations do not model the cold gas phase, this has the result the gas temperature at star formation reflects the effective pressure imposed on the interstellar medium (ISM).
- Stellar mass loss and metal enrichment: Star particles are considered to be simple stellar populations, where the number of stars reaching the end of the main sequence can be calculated. This, together with the initial elements abundances, gives the information of the emitted mass, which is distributed along the neighboring SPH particles.
  The stars inherit the smoothed-kernel abundances from the gas particles and this is used to calculate the lifetimes and yields.
- Energy feedback from star formation: Here, the energy feedback from star formation is stochastic thermal feedback, instead of kinetic feedback.
- The accretion into black holes accounts for angular momentum (this is not important in our case since we are assuming there is no black hole).

3.3 Parameters

The parameters to change between the different simulations will be the following ones:

- Fraction of gas (f_{gas}): This parameter is actually one of the initial conditions, not of the parameter file. Its meaning is the fraction from the total mass that comes in the way of gas particle. We assume for the standard model that not all baryons are accreted into such a low mass halo, choosing a value that is motivated by cosmological simulations e.g. Christensen et al. 2016 [6].
  Standard value: $f_{gas} = 0.1$
- Delay time of supernova of type II: The time it takes for the feedback energy to by released.
  Standard value: $delay = 30\ Myr$
- Star formation efficiency: This is controlled by changing the feedback produced by star formation, as establish in Schaye and Dalla Vechia (2008) [32], by changing the parameter A from the Kennicutt-Schmidt star formation law.
  Standard value: $A = 1.191 \times 10^{-4}\ M_{\odot}\ yr^{-1}\ kpc^{-2}$
- Equation of state: It gives the relation between pressure and density, $P_{EOS} \propto \rho^{\gamma}$. There are three parameters that can change the equation of state:
  - The threshold density: This controls where the ideal equation of state is used, it is the upper limit in density.
  - Gas temperature at the threshold density, .
  - γ: This is the slope of the EoS (the polytropic index). This value should not be changed since it could cause spurious fragmentation, right now is avoided because the value 4/3 makes the Jeans mass independent of the density.

  Here we will change the threshold density, increasing its value will give a smaller pressure in the center. Standard value: $n_{H,min} = 0.1\ cm^{-3}$
- Star formation density threshold: If the previous controlled the pressure, this one controls the star formation, for densities higher than this the cold phase needed for star formation is expected to form.
  Standard value: $n_H = 0.1\ cm^{-3}$
- Resolution: By changing the number of particles we can get a different resolution.
  Standard value: $n_{dm} = 1 \times 10^5, \quad n_{gas} = 1 \times 10^5$
- SNII heating temperature: This controls the numbers of particles heated by each SNII explosion.
  Standard value: $T_{SN} = 10^{7.5}\ K$

The values for the different simulations are the ones shown in Table 1.

id	n_{dm}	n_{gas}	f_{gas}	Delay time (Myr)	A ($M_\odot\ yr^{-1}\ kpc^{-2}$)	$n_{H,EOS}$ (cm^{-3})	$n_{H,SF}$ (cm^{-3})	$T_{SN}(K)$
1	10^5	10^5	0.1	30	1.191×10^{-4}	0.1	0.1	$10^{7.5}$
2	10^5	10^5	0.1	**0**	1.191×10^{-4}	0.1	0.1	$10^{7.5}$
3	10^5	10^5	**0.16**	30	1.191×10^{-4}	0.1	0.1	$10^{7.5}$
4	10^5	10^5	**0.16**	**0**	1.191×10^{-4}	0.1	0.1	$10^{7.5}$
5	10^5	10^5	0.1	30	$\mathbf{1.515\times10^{-4}}$	0.1	0.1	$10^{7.5}$
6	10^5	10^5	0.1	30	1.191×10^{-4}	**1**	0.1	$10^{7.5}$
7	10^5	10^5	0.1	30	1.191×10^{-4}	0.1	**1**	$10^{7.5}$
8	10^5	10^5	0.1	30	1.191×10^{-4}	**1**	**1**	$10^{7.5}$
9	10^5	10^5	0.1	30	1.191×10^{-4}	**10**	0.1	$10^{7.5}$
10	10^5	10^5	0.1	30	1.191×10^{-4}	0.1	**10**	$10^{7.5}$
11	10^5	10^5	0.1	30	1.191×10^{-4}	**10.0**	**10**	$10^{7.5}$
12	10^5	10^5	**0.16**	30	1.191×10^{-4}	**10**	0.1	$10^{7.5}$
13	10^5	10^5	**0.16**	30	1.191×10^{-4}	0.1	**10**	$10^{7.5}$
14	10^5	10^5	**0.16**	30	1.191×10^{-4}	**10**	**10**	$10^{7.5}$
15	10^5	10^5	0.1	30	1.191×10^{-4}	**100**	**10**	$10^{7.5}$
16	10^5	10^5	0.1	30	1.191×10^{-4}	**100**	**10**	$\mathbf{10^7}$
17	10^5	10^5	**0.16**	30	1.191×10^{-4}	**100**	**10**	$10^{7.5}$
18	10^5	10^5	**0.16**	30	1.191×10^{-4}	**100**	**10**	$\mathbf{10^7}$
19	10^5	10^5	**0.16**	**0**	1.191×10^{-4}	**100**	**10**	$10^{7.5}$
20	$\mathbf{10^6}$	$\mathbf{10^6}$	0.1	30	1.191×10^{-4}	0.1	0.1	10^7

Table 1: Values of the parameters for the different runs of the simulation. The first row corresponds to the standard values, for the rest of the runs the values changed are bolded. Here, an id is established for each simulation for future reference.

3.4 Analysis

Star Formation History

To analyze the SFH we integrate the output obtained directly from gadget. This output gives different types of measures for the star formation rate for each time step, we will use the total solar masses formed per year.

However, just plotting this data is too noisy to give a general idea of the real SFH, so we integrated over 149 time bins, to get a smoothed plot.

Dark matter density profile

We are interested in the density profile at the final time of the simulation and the deviations from a NFW profile [20], this profile consists on the mean density of each layer as a function of radius. To check this we need to compute the density profile the same way they did, assuming spherical layers, even though there is not perfect spherical symmetry. To do the fit we stay below R200 (the radius within which the density is $200 \times \rho_{crit}$).

The fit is done in the log-log plane to a NFW profile (eq. 47).

$$\rho = \frac{\rho_0}{\frac{r}{r_s}\left(1+\frac{r}{r_s}\right)^2} \tag{47}$$

where r_s is the scale radius.

Gas mass

Here, the aim is to be able to see if there are inflows and outflows taking place. To know this we add up, for each time step, the mass of all gas that has a radius lower than 1 kpc and lower than 2 kpc from the central regions of the simulated galaxies where core formation may occur.

4 Analysis of the results

After running all of the simulations with the different parameters we are going to compare them, see what are the changes, and check if we were able to get a profile different than the NFW, specially if we get a profile with a core.

4.1 Star Formation History

The SFH give us an idea of the evolution of the galaxy and we can check if it looks realistic. We see the following behaviour: First, everything collapse to the center, causing the first outburst of star formation, this happens soon after the simulation begins; then, the feedback generated should decrease the star formation, but, since the galaxy is still collapsing, the star formation should increase again soon after that, and be slowed by feedback again; giving a bursty SFH. Once the collapse is over we expect the star formation to decrease steadily since the galaxy is isolated and, therefore, there cannot be any inflows that cause more star formation.

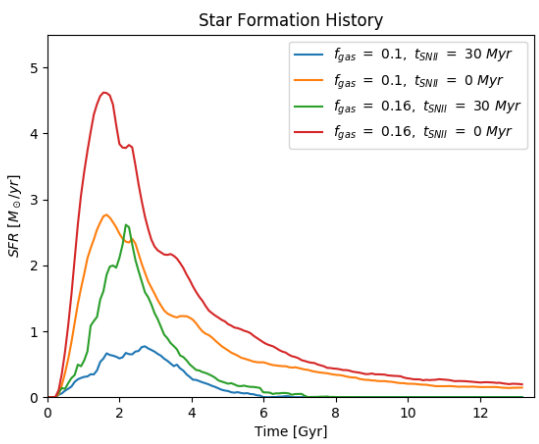

(a) Parameters f_{gas} and t_{SNII}.

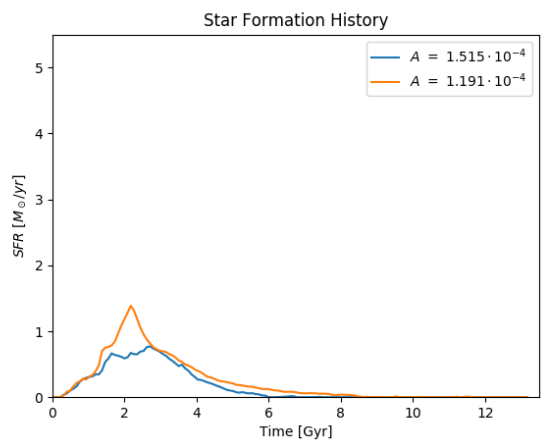

(b) Star formation efficiency.

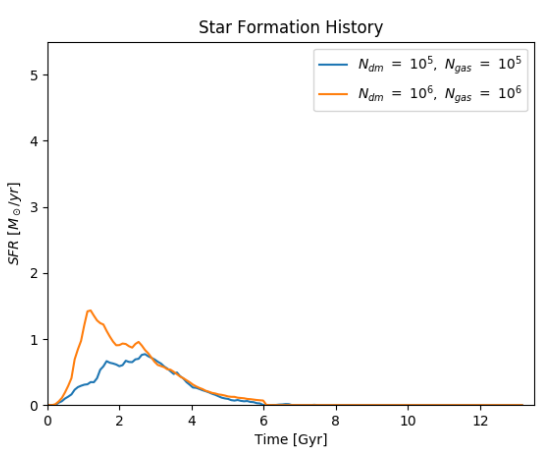

(c) Number of particles (resolution)

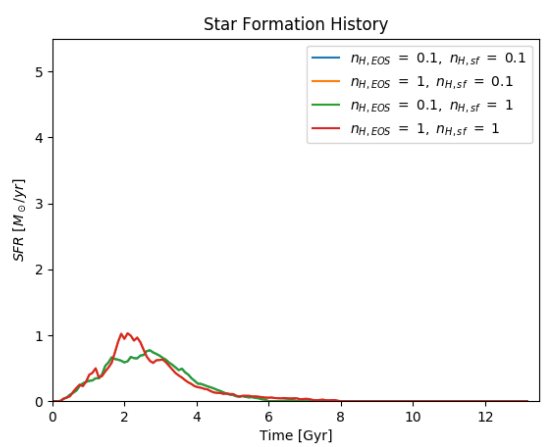

(d) Density thresholds (the green and red lines overlap the blue and the orange lines respectively).

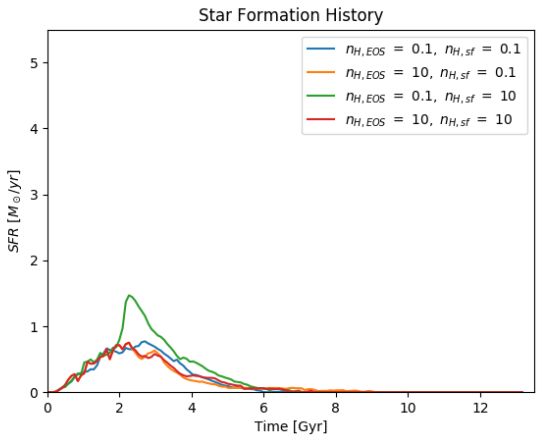

(e) Density thresholds.

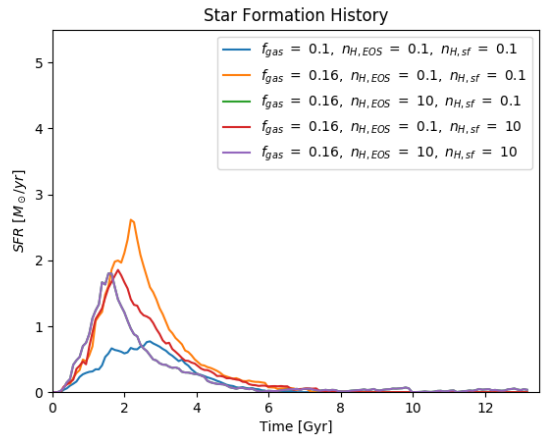

(f) Both f_{gas} and density thresholds.

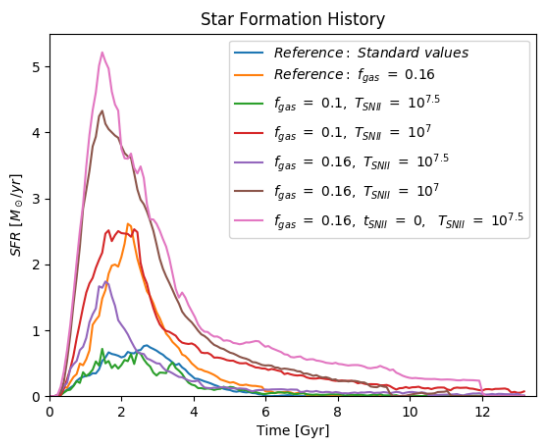

(g) f_{gas} and the temperature of SNII, with $n_{H,EOS} = 100cm^{-3}$ and $n_{H,sf} = 10cm^{-3}$.

Figure 3: SFH of the different runs of the simulation, grouped by the parameters changed in each run (simulations with different density threshold are grouped in more than one plot for clarity). Note that the first series of each plot (blue line) has the considered standard values for comparison.

Note that the blue line in each of the plots in Figure 3 is the reference simulation. The parameter values for this case are stated in the first row of Table 1.

Unexpectedly, making t_{SNII} zero results in a higher star formation rate (Figure 3a), which is only reached in the simulation with high density thresholds and lower SNII temperature. However, the shape of this series are not exactly what we expected, they become more smoothed, instead of the expected bursty star formation. This increase in the star formation rate also happens when the gas fraction is larger, as should be expected, and the otherwise behaviour of the SFH is similar.

As for the SFH for the different values of star formation efficiency, which increases for a smaller value of A (Figure 3b), being A the normalization of th Kennicut-Schmidt law, results in a peak

of star formation, completely removing the bursty shape. Although this peak is smaller than the ones obtained for different values of f_{gas} and t_{SNII}, the shape of it indicates the contribution of the feedback is not able to stop the star formation.

Changing the resolution (by increasing the number of particles, Figure 3c) results in a peak of star formation that happens sooner than the other runs. It also gets slightly less bursty. But the most interesting thing is that the peak happens sooner than all the other cases, which means that the collapse is happening faster.

We now change the values of the density threshold (Figures 3d, 3e and 3f), this is grouped in three sets, one with a small change in both density thresholds (from 0.1 to 1), one with a larger variation (from 0.1 to 100) and another one where also f_{gas} is changed. We can see in Figure 3d that a small change in the density threshold for the equation of state slightly change the SFH, increasing a little the peak of star formation, but keeping the overall behaviour. However, the change in the density threshold for the star formation does not change the SFH at all (the results overlap in the picture).

A larger increase in $n_{H,sf}$, does change the profile, resulting in a "peaky" SFH. However, this faces away when $n_{H,EOS}$ is also changed, showing that for equal values of the density threshold the behaviour is dominated by the density threshold stablish for the star formation. It seems that increasing the initial gas fraction enforces this dominance of the equation of state over the star formation, since the profiles overlap for whatever value $n_{H,sf}$ has, whenever $n_{H,EOS}$ is the same; anyway, the effect of the different values of the star formation is less important, since the profile is clearly affected by the value of f_{gas}, although the peak with this thresholds is lower.

When the value of $n_{H,EOS}$ gets even larger (Figure 3g) the profile gets more bursty, however, this behaviour is canceled when we decrease the SNII temperature, resulting in a peak in star formation. This can also be seeing in the case where the initial gas fraction is 0.16; also, when t_{SNII} is null the peak gets larger, but some bursty behaviour can be seen when the SFH is decreasing.

4.2 Navarro, Frenk and White profile

There are two interesting things to check here, how each of the runs fit to a NFW profile (Figure 4), since we would like to see what parameters are able to break this profile, and also, how different the density profiles are from one simulation to another, to make the comparison easier (Figure 5).

Here we check possible deviations from the NFW profile in the central part of the halo. All the plots are in Figure 4, and a comparison between the different runs (grouped by the parameters changed) are in Figure 5. First, we can see from our standard case that the innermost regions are not perfectly fit with the NFW profile, but that is due to the resolution, since it gets worse por radius lower than $\sim 0.3kpc$, which is approximately the softening length (0.332 kpc). And even when the fit gets worse it does not have a flat core. This is not changed by an increase in the initial fraction of gas (Figure 4c)

When we decrease t_{SNII} for supernova of type II, however, the profile gets much more flat for radius lower than 1kpc; this is specially obvious in Figure 4d.

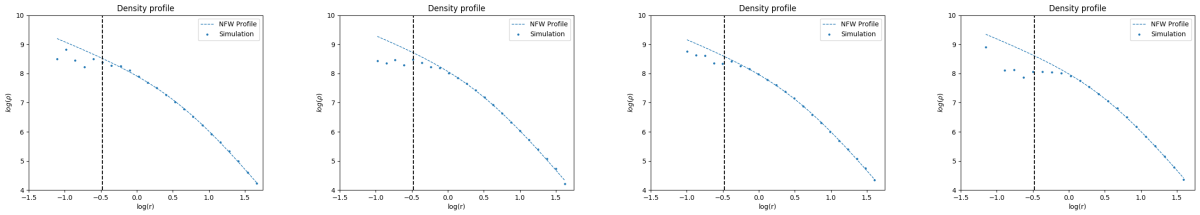

(a) id: 1

(b) id: 2

(c) id: 3

(d) id: 4

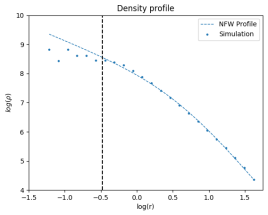

(e) id: 5

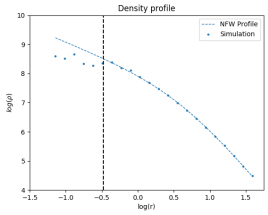

(f) id: 6

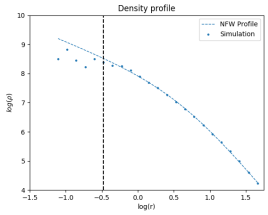

(g) id: 7

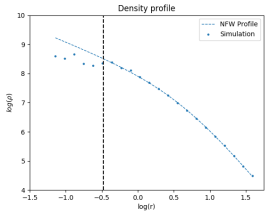

(h) id: 8

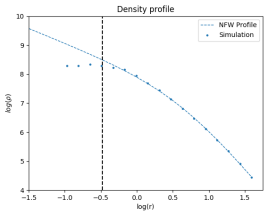

(i) id: 9

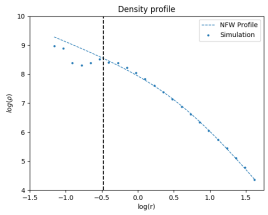

(j) id: 10

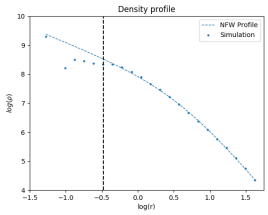

(k) id: 11

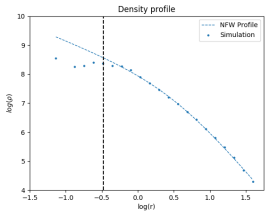

(l) id: 12

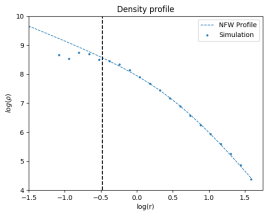

(m) id: 13

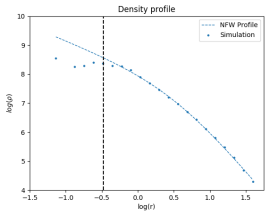

(n) id: 14

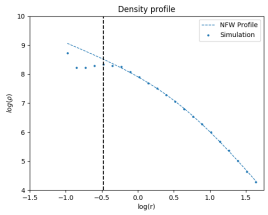

(o) id: 15

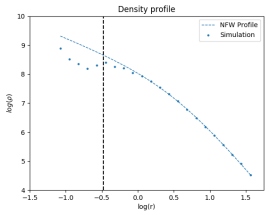

(p) id: 16

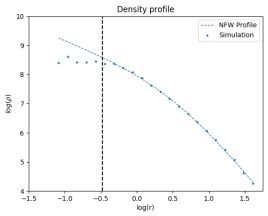

(q) id: 17

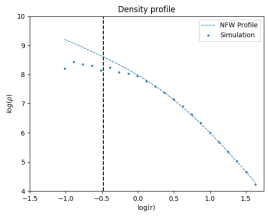

(r) id: 18

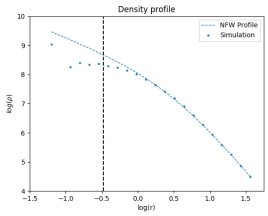

(s) id: 19

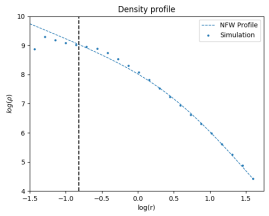

(t) id: 20

Figure 4: Density profile and its fit to a Navarro, Frenk and White profile for the different simulations, from left to right and top to bottom, following the same order as Table 1. The real profile is represented as the scatter plot and the dashed line is the best fit to the NFW profile. The red lines indicates the softening length.

The behaviour for different star formation efficiencies [Figure 4e] is really similar, high density in the central parts when star formation is higher, and a slightly less cuspy profile.

For the density threshold for star formation, the effects are only visible when the value is high enough, and even then the profile is not flat. However, the density threshold for the equation of state does flatten the profile, specially for higher values; also, this parameter dominates over $n_{H,sf}$, although the effects of $n_{H,sf}$ are noticed when it takes the value 10 cm^{-3}. The results are less obvious when $f_{gas} = 0.16$, but the profiles change the same way.

Decreasing the temperature of the SNII does not seem to flatten the profile, however, the combination of initial fraction of gas higher and lower SNII temperature results in a flat profile, although it gets flats at a radius too close to the resolution limit. This does not happen when t_{SNII} is null, and the density in the central regions is higher.

Changing the resolution does not seem to affect the formation of a core, since the profile is nicely fit by a NFW profile.

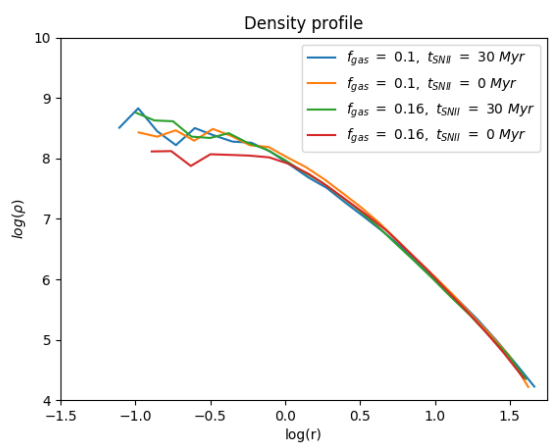

(a) Different initial fraction of gas and t_{SNII}.

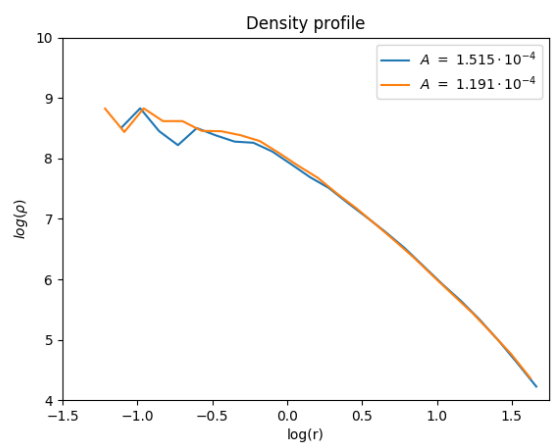

(b) Different star formation efficiency.

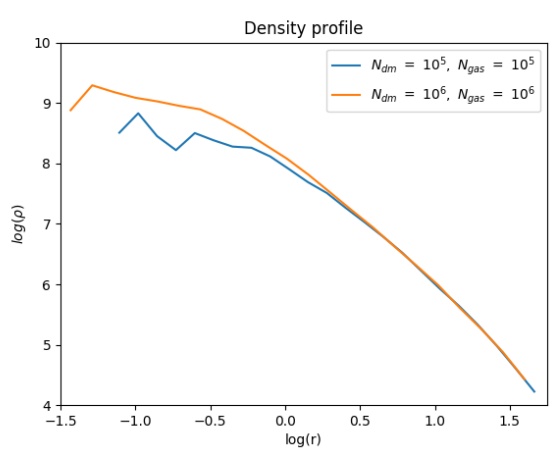

(c) Resolutions (number of particles).

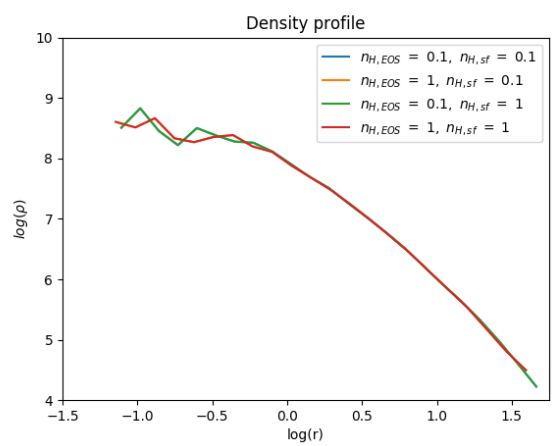

(d) Density threshold up to 1 (the green and red lines overlaps the blue and orange lines respectively).

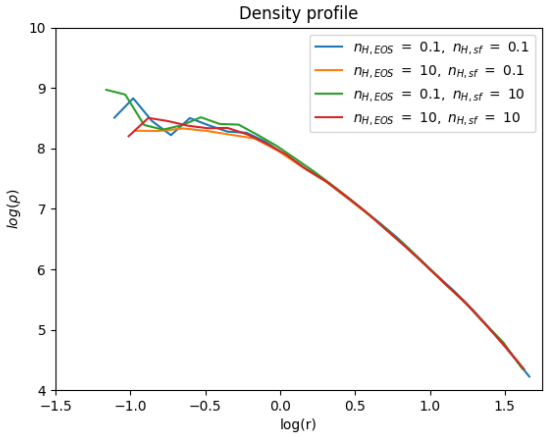

(e) Density threshold with range $0.1 - 10$.

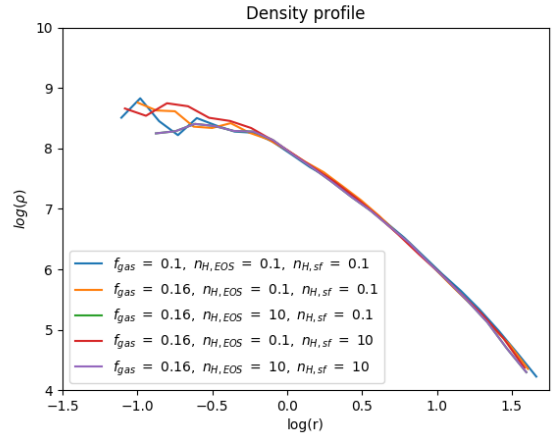

(f) $f_{gas} = 0.16$. Density threshold with range $0.1 - 10$

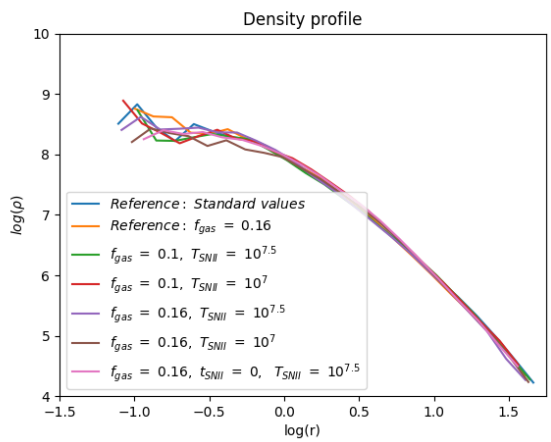

(g) Different fractions of gas and SNII temperature with $n_{H,EOS} = 100\ cm^{-3}$ and $n_{H,sf} = 10\ cm^{-3}$.

Figure 5: Comparison of density profiles for the different simulations grouped by the parameters changed in each run.

4.3 Gas mass in the innermost regions

This can give us information about inflows and outflows of gas from the center, since the gas mass can change either because of the star formation (consuming part of the gas), or because it is moving to of from the outer parts. This can be interesting since one of the theories states that cusp-core transformation can be given by gas outflows.

In figure 6 we show the gas mass within 1 kpc (solid) and 2kpc (dashed) of the centre of the simulated galaxies. Here we can see that, first, the gas falls to the center, which activates the star formation. Then, it gets used up and ejected to the outer layers. We would expect to be subsequent inflows and outflows of gas, but for most of these parameters the gas just changes smoothly, by flowing to the outer layers or being used in star formation. There are signs of inflows and outflows for the run with highest density threshold while keeping the fraction of gas and the temperature

of SNII as the standard values (Figure 6g). However, others works show that density thresholds around 10 are enough to have inflows and outflows, this may be related to the way the energy is distributed after supernova explosions, in this code a lot of energy is put into a small number of particles, but this changes when we decrease T_{SNII}, and we cannot see these flows of gas. The behaviour is similar with 30 Myr of delay time or without delay.

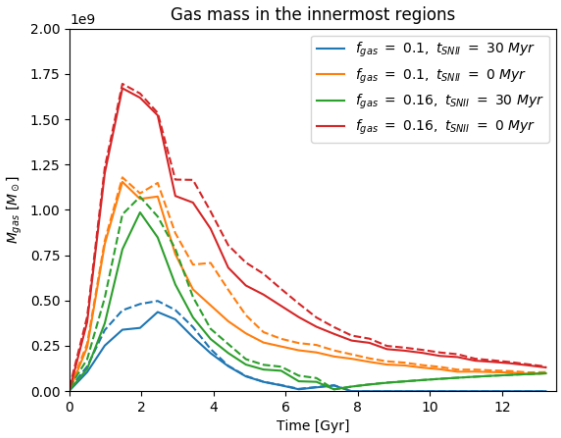

(a) Runs with different fraction of gas and t_{SNII}. The solid line goes for the inner 1 kpc, and the dashed line for the inner 2 kpc.

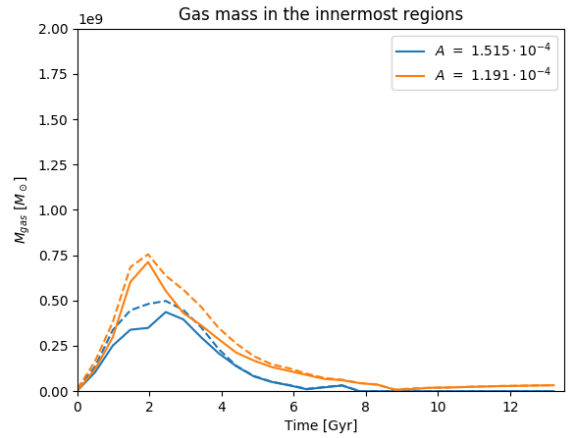

(b) Runs with different star formation efficiency. The solid line goes for the inner 1 kpc, and the dashed line for the inner 2 kpc.

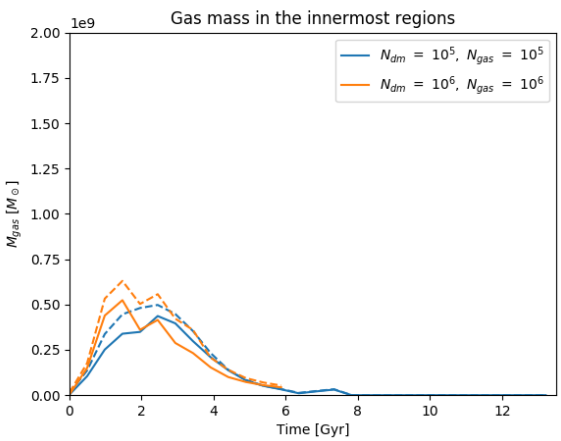

(c) Runs with different resolution (number of particles. The solid line goes for the inner 1 kpc, and the dashed line for the inner 2 kpc.

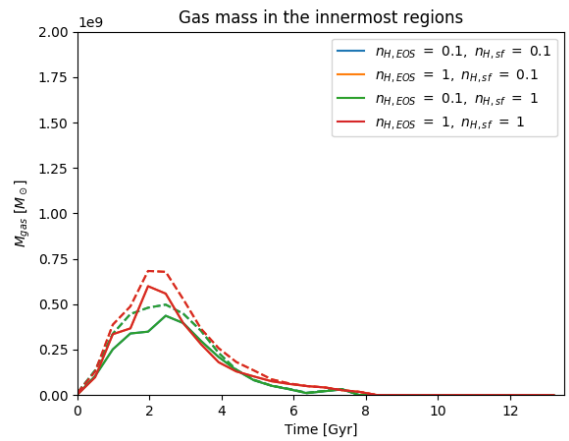

(d) Runs with slightly different density thresholds. The solid line goes for the inner 1 kpc, and the dashed line for the inner 2 kpc (the green and red lines overlaps the blue and the orange lines respectively).

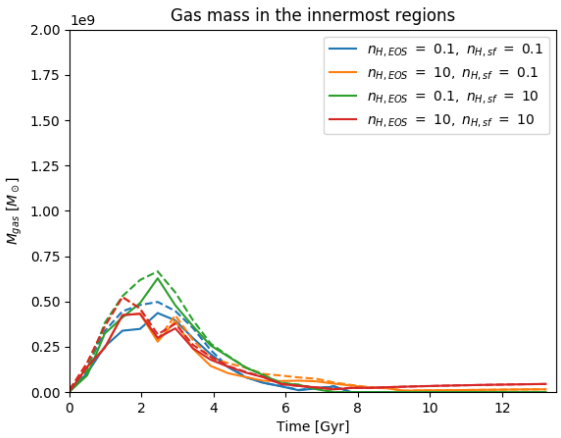

(e) Runs with a large difference in the density thresholds. The solid line goes for the inner 1 kpc, and the dashed line for the inner 2 kpc.

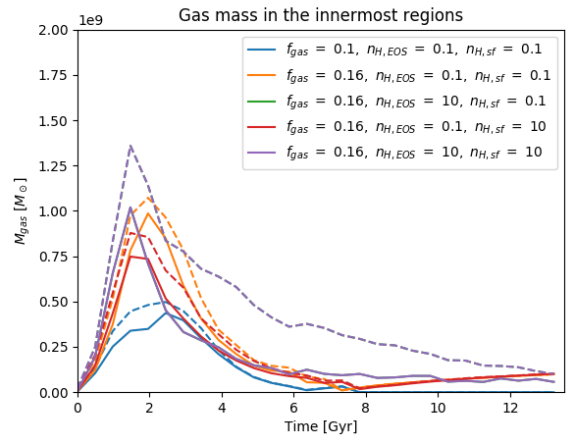

(f) Runs with different fraction of gas and density thresholds. The solid line goes for the inner 1 kpc, and the dashed line for the inner 2 kpc.

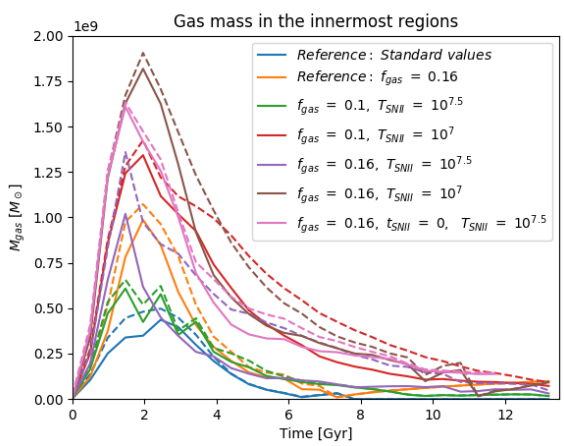

(g) Runs with different fraction of gas and SNII temperature. The solid line goes for the inner 1 kpc, and the dashed line for the inner 2 kpc.

Figure 6: Gas mass in the innermost regions of the galaxy for the different simulations. The solid line goes for the inner 1 kpc, and the dashed line for the inner 2 kpc.

4.4 Stellar density profile

Here we analyze the stellar distribution, we can see that the effect of the different parameters over this feature is not as big as the previous ones. The shape is approximately the same for all simulations, we can see a bulge in the innermost regions (a flatten profile), with a exponential fall in the outer layers.

What changes from one simulations to another is the size of the bulge and the total stellar mass.

For example, the simulation with $f_{gas} = 0.16$ and $t_{SN} = 0\ Myr$ has almost no bulge, while the case with $n_{H,sf} = 10\ cm^{-3}$ and $n_{H,EOS} = 0.1\ cm^{-3}$ has a bulge that extends to 0.5 kpc. The differences in the total stellar mass are explained by the different SFHs. The galaxy formed from the simulation with highest density thresholds and no delay time seems to be more concentrated in the central regions, with the density profile falling rapidly, it was also the one with the highest concentration of dark matter in the center.

Comparing these with the dark matter density profiles it seems that galaxies with a bulge has a tendency to follow a NFW profile, whether the profiles where there is no bulge or is the smallest are the ones that seem to have a dark matter core. This can be because the higher star formation in the center deepens the potential, preventing the galaxy from forming a dark matter core.

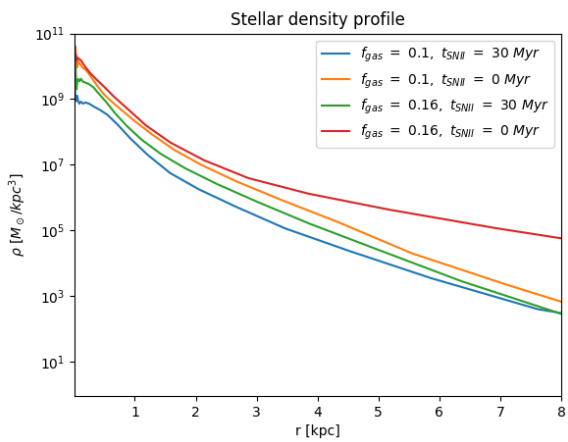

(a) Runs with different fraction of gas and t_{SNII}.

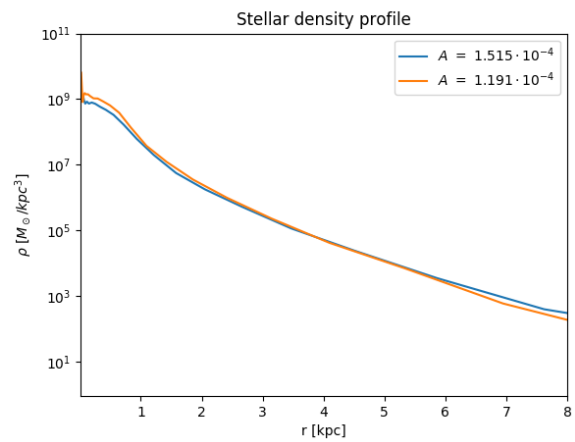

(b) Runs with different star formation efficiency.

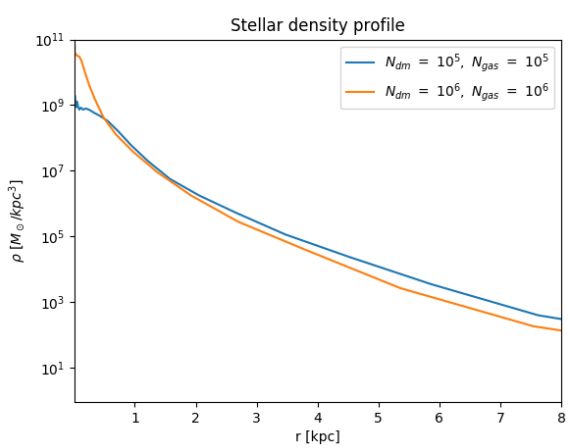

(c) Runs with different resolution (number of particles.

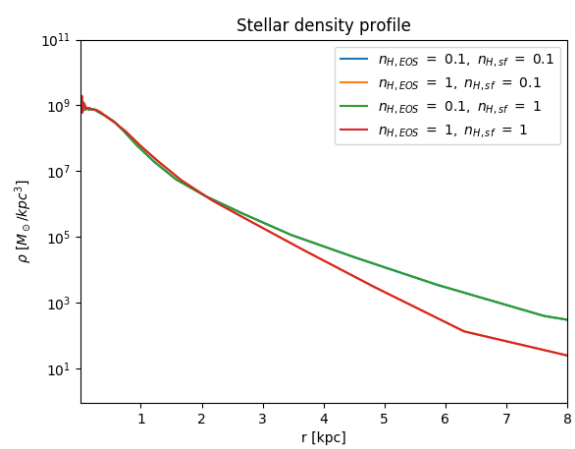

(d) Runs with slightly different density thresholds (the green and red lines overlaps the blue and the orange lines respectively).

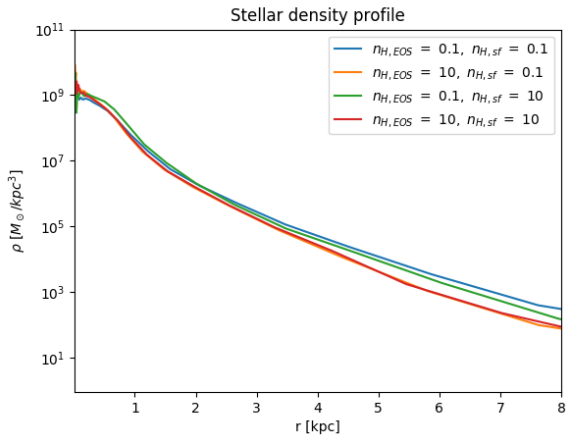

(e) Runs with a large difference in the density thresholds.

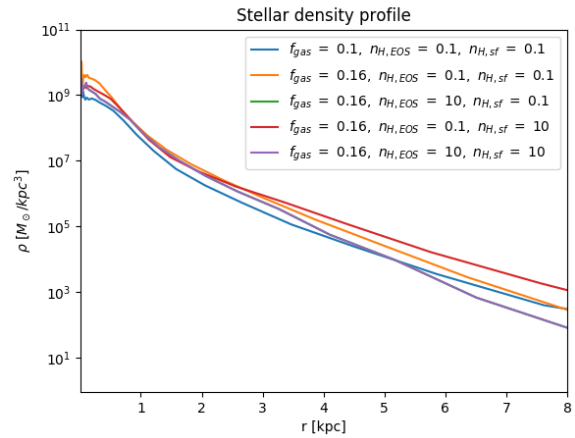

(f) Runs with different fraction of gas and density thresholds.

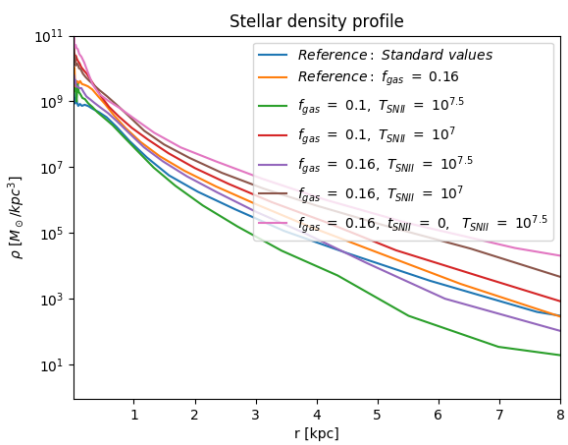

(g) Runs with different fraction of gas and SNII temperature and with $n_{H,EOS} = 100\ cm^{-3}$ and $n_{H,sf} = 10\ cm^{-3}$.

Figure 7: Stellar density profile for the different simulations grouped by the parameters changed in each run.

4.5 Mass relations

Since we begin with the same initial mass, we can expect the total mass to be the same for all of our galaxies. But this is not true for the stellar or mass, since star formation it is different in each simulations, as we saw.

As it is expected galaxies with the highest star formations rates end up with the highest stellar mass and the lowest gas mass. Apart from this two values there are two clear tendencies in Figure 8c, which are grouped by the initial fraction of gas. In Figures 8a and 8b we can see the simulations ordered by the stellar mass and gas mass, respectively, and we can see that the total mass of the galaxy (M_{200}) is slightly larger that what we set in the initial conditions (we end up with a galaxy of $6 \cdot 10^{10}$ $M_\odot$ instead of $5 \cdot 10^{10}$ $M_\odot$), this is due to the calculations done when generating the initial conditions.

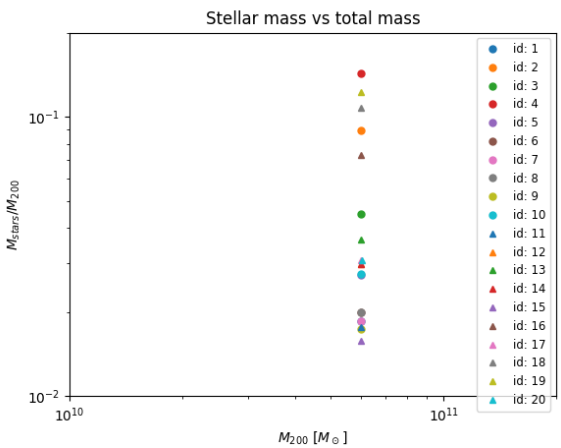

(a) Relation between stellar mass and total halo mass for all galaxies.

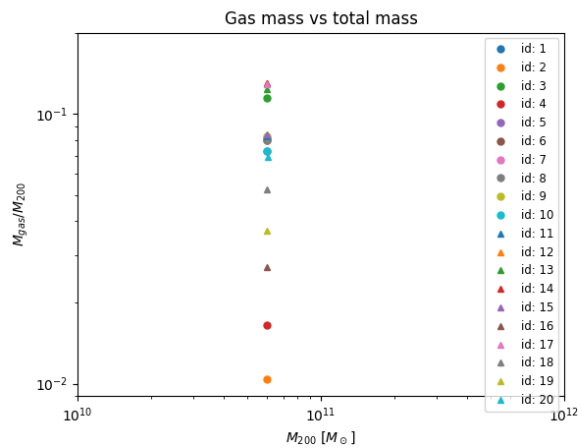

(b) Relation between gas mass and total halo mass for all galaxies

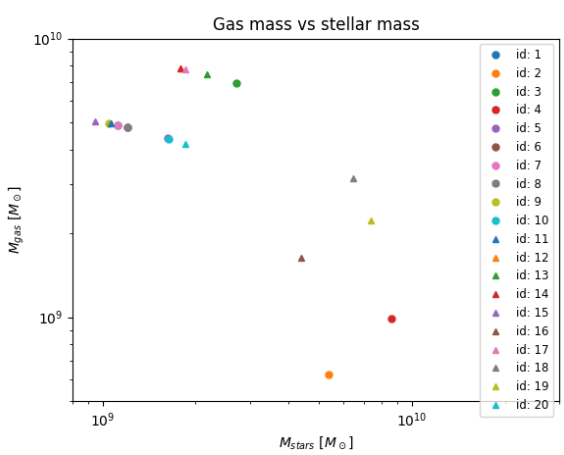

(c) Relation between gas mass and stellar mass for all galaxies.

Figure 8: Mass relations for different components for all the simulations

5 Conclusions

Several groups have found that cores can form within galaxy formation simulations that include baryons and the effects of feedback. For example, Governato et al. 2010 [9] and Pontzen and Governato 2014 [26] find cores formed by outflows of gas, whilst Di Cintio 2014 [7] find a dependence of core formation on the ratio of stellar to halo mass, as did Chan, Keres, Oñorbe et al. 2015 [5] whilst Read, Agertz and Collins 2016 [28], also found a dependence of core formation on star formation rate. By contrast, simulations run with the EAGLE code have generally found cuspy dark matter density profiles, even when baryons are included (see Sawala et al. 2016).

These EAGLE simulations, in general, have a relatively smooth SFH, compared to the behaviour observed in other simulations e.g. Di Cintio et al. 2014 [7]. We do know that a bursty star formation driving gas outflows is important in core formation models within cosmological simulations (e.g. Pontzen & Governato 2014 [26]). We endeavored to understand the differences between the EAGLE model and these other models that form cores. We did this by changing a range of parameters of the EAGLE model and testing their effects on core formation. We found that the changes observed when modifying the parameters were not dramatic. Looking at the star formation history, we saw that:

- The effects of modifying parameters such us the star formation efficiency, density threshold for star formation and the delay time and the temperature of SNII results in a large peak of star formation and the behaviour of star formation remains smooth rather than bursty.
- The effect of increasing $n_{H,sf}$, the density threshold for star formation, is minimal when the density threshold for the equation of state is equal or higher.
- A high value of $n_{H,EOS}$, i.e. retaining an ideal equation of state at higher densities, does result in a slightly more bursty star formation rate although it remains relatively smooth compared to other models such as FIRE simulations (Chan et al. 2016 [5]).
- Increasing the initial fraction of gas increases the star formation peak and when we combine this with variation of the density threshold the profiles get smoother than other simulations with the same values for the density thresholds.
- The effect of increasing the resolution is that the star formation peak happens earlier.

The case with a more bursty star formation history resulted in more outflows and a flatter profile. This effect was quite small in the EAGLE simulations, however. The biggest difference is made when we change the delay time of SNII feedback. When there is a delay between forming stars and providing feedback, the galaxy is stable to core formation, which can be because stars add to the potential well before gas is ejected, and then the changes in the potencial are less dramatic. Another interesting parameter is the temperature of SNII, in EAGLE this temperature is high to avoid artificial cooling, but this has the effect that a few particles are heated to a high temperature, instead of spreading the energy around more, like they do in other models where a large number of particles are heated to a lower temperature. This means that, in EAGLE, less mass is being ejected during star formation, then, the processes that create cores are not taking place; this is consistent with the gas mass plots.

Also, the formation of a bulge seems to be related to the dark matter profile, preventing the dark matter to form a core. This is because the formation of stars in the inner region has deepened the

potential well, making core formation more difficult. This is perhaps why the delay in supernova feedback was the most important parameter in our study. With a 30 Myr delay in supernova feedback, stars are able to form in this period which adds to the potential and minimizes changes in the potential when feedback finally occurs. We do know that the supernova feedback is delayed in star forming regions. This may be interpreted as requiring other forms of stellar feedback, which occur prior to supernova energy, to form cores. In EAGLE this stellar feedback is modeled by the change in equation of state, which proves a pressure in star forming regions. Our simulations indicate that this type of feedback does not transform cusps into cores.

As mentioned, the standard EAGLE simulations find no cores, just as we can see in the standard case in our simulation, that shows a nice NFW fit. We have seen that parameters such as the delay time for SNII, the density threshold for the equation of state and the resolution are able to obtain a profile slightly different than NFW, with a small core being formed in the center regions, which correspond to simulations with a slightly more bursty star formation; but there is not a huge difference for any set of parameters. Moreover, when we use parameters similar to those of Di Cintio et al. 2014 [7] or Chan et al. 2016 [5] the simulations still do not form a core, whilst theirs do, we also observe no sign of inflows and outflows, whilst their simulations present these movements of gas. Also, even when cores are formed, they are significantly smaller than the ones formed in other simulations, Di Cintio et al. 2014 [7], Governato et al. 2010 [9], Pontzen & Governatio 2014 [26], Read et al. 2016 [29] and Chan et al. 2016 [5].

So in the end we can conclude that the most important difference between EAGLE code and others is the SN feedback prescriptions, as well as the way that feedback from stars is implemented, rather than the star formation prescriptions or the equation of state (which can prevent to much gas falling to the center, and the core formation processes require gas falling to the center and then being expelled).

References

[1] Barschel, Colin, *Structure formation in the Universe*, Aachen University of Technology, (July 13, 2007).

[2] Bertschinger, E., *Self-similar secondary infall and accretion in an Einstein-de Sitter universe*, Astrophysical Journal Supplement Series (ISSN 0067-0049), vol. 58, May 1985, p. 39-65 (1985)

[3] Blumenthal, George R., et al., *Formation of galaxies and large-scale structure with cold dark matter*, Nature volume 311, pages 517–525 (1984)

[4] Bullock, James S., and Boylan-Kolchin, Michael, *Small-Scale Challenges to the CDM Paradigm*, Annual Review of Astronomy and Astrophysics, vol. 55, pp. 343-387 (2017).

[5] Chan, T. K., Keres, Onorbe, J. et al., *The impact of baryonic physics on the structure of dark matter haloes: the view from the FIRE cosmological simulations*, MNRAS, Volume 454, pages 2981–3001 (2016).

[6] Christensen, Charlotte R., *In-N-Out: The Gas Cycle from Dwarfs to Spiral Galaxies*, Hamilton, ON L8S 4L8, Canada) ApJ, Volume 824, Issue 1, article id. 57, 19 pp. (2016).

[7] Di Cintio, Arianna et al., *The dependence of dark matter profiles on the stellar-to-halo mass ratio: a prediction for cusps versus cores*, MNRAS, Volume 437, Issue 1, p.415-423 (2014)

[8] El-Zant, Amr, Shlosman, Isaac, & Hoffman, Yehuda, *Dark Halos: The Flattening of the Density Cusp by Dynamical Friction*, ApJ (2001)

[9] Governato et al, *At the heart of the matter: the origin of bulgeless dwarf galaxies and Dark Matter cores*, Nature, Volume 463, pp. 203-206, (2010).

[10] Hamilton, A. J. S., *Formulae for Growth Factors In Expanding Universes Containing Matter and a Cosmological Constant*, (February 1, 2008).

[11] Hernquist, Lars, *An analytical model for spherical galaxies and bulges*, ApJ, Part 1, vol. 356, pp. 359-364 (1990)

[12] Hoffman, Yehuda, *On the formation and structure of galactic halos*, ApJ, Part 1 (ISSN 0004-637X), vol. 328, pp. 489-498 (1988)

[13] Hunter, D. A. et al, *Little Things.*, AJ 144, 134 (2012).

[14] Kuzio de Naray, R. and Spekkens, K., *Do Baryons Alter the Halos of Low Surface Brightness Galaxies?*, ApJ 741, L29 (2011).

[15] Mo, H. J., Mao, Shude, and White, Simon D. M., *The formation of galactic disks*, MNRAS, Volume: 295, (1997).

[16] Mardoff Nielsen, Robert, *Master thesis: Spherical Collapse in Dark Energy Models*, Institute of Theoretical Astrophysics, University of Oslo, (June 1, 2011).

[17] Mashchenko, Sergey et al., *The removal of cusps from galaxy centres by stellar feedback in the early Universe*, Nature, Volume 442, Issue 7102, pp. 539-542 (2006).

[18] Moore, Ben, *Evidence against dissipation-less dark matter from observations of galaxy haloes*, Nature, Volume 370, Issue 6491, pp. 629-631 (1994).

[19] Navarro, Julio F., et al., *The cores of dwarf galaxy haloes*, MNRAS, Volume 283, Issue 3, pp. L72-L78. (1996)

[20] Navarro, Julio F., Frenk, Carlos S., and White, Simon D.M., *A Universal Density Profile from Hierarchical Clustering*, ApJ, (1997).

[21] Navarro, Julio F., Frenk, Carlos S., and White, Simon D.M., *Simulations ofX-ray clusters*, MNRAS 275, 720-740 (1995)

[22] Newman, A. B., Treu, T., Ellis, R. S. & Sand, D. J., *The Density Profiles of Massive, Relaxed Galaxy Clusters. II. Separating Luminous and Dark Matter in Cluster Cores.*, ApJ 765, 25 (2013).

[23] Oh, Se-Heon, et al., *THE CENTRAL SLOPE OF DARK MATTER CORES IN DWARF GALAXIES: SIMULATIONS VERSUS THINGS0*, AJ 142, 1 (2011).

[24] Planck Collaboration et al., *Planck 2013 results. XVI. Cosmological parameters.*, A&A (2013).

[25] Percival, W. J. et al., *The 2dF Galaxy Redshift Survey: the power spectrum and the matter content of the Universe.*, MNRAS 327, 1297– 1306 (2001).

[26] Pontzen, Andrew, and Governato, Fabio, *Cold dark matter heats up*, Nature, 506, 171 - 178 (13 Feb 2014).

[27] Power, C. et al. *The inner structure of ΛCDM haloes - I. A numerical convergence study*, MNRAS 338, Issue 1, pp. 14-34. (2003).

[28] Read, J. I., Agertz, O., Collins, M. L. M., *Dark matter cores all the way down*, MNRAS, Volume 459, Issue 3, pages 2573–2590 (2016)

[29] Read, J. I., Pontzen, A. P. and Viel, M., *On the formation of dwarf galaxies and stellar haloes*, MNRAS 371, Issue 2, pp. 885-897 (2006).

[30] Ries, Adam G. et al., *Observational Evidence from Supernovae for an Accelerating Universe and a Cosmological Constant*, Astron.J. 116: 1009-1038 (1998)

[31] Sawala, Till, *The APOSTLE simulations: solutions to the Local Group's cosmic puzzles*, MNRAS, Volume 457, Issue 2, p.1931-1943 (2016)

[32] Schaye, Joop, and Dalla Vecchia, Claudio, *On the relation between the Schmidt and Kennicutt-Schmidt star formation laws and its implications for numerical simulations* MNRAS, Volume: 383, page: 1210, (2008).

[33] Schaye, Joop, et al., *The EAGLE project: Simulating the evolution and assembly of galaxies and their environments*, MNRAS, 446, 521, (2015).

[34] Springel, Volker, *The cosmological simulation code GADGET-2*, MNRAS, Volume 364, Issue 4, pp. 1105-1134, (2005).

[35] Walter, F., et al., *THINGS: The HI Nearby Galaxy Survey* AJ 136, 2563–2647 (2008).